Interreg Alpine Space project - **NEWFOR**

Project number 2-3-2-FR

NEW technologies for a better mountain **FOR**est timber mobilization

Priority axis 2 - Accessibility and Connectivity

Workpackage 4: Forest resources and LiDAR

A Review of Surface Roughness Concepts, Indices and Applications

- Sate of the Art -

Coordinator(s): Markus Hollaus (Vienna University of Technology – Austria, Department of Geodesy and Geoinformation, Research Group for Photogrammetry (E120-7))
Contributors: Milutin Milenković (Vienna University of Technology – Austria, Department of Geodesy and Geoinformation, Research Group for Photogrammetry (E120-7)); Norbert Pfeifer (Vienna University of Technology – Austria, Department of Geodesy and Geoinformation, Research Group for Photogrammetry (E120-7))

Final version 30/November/2014

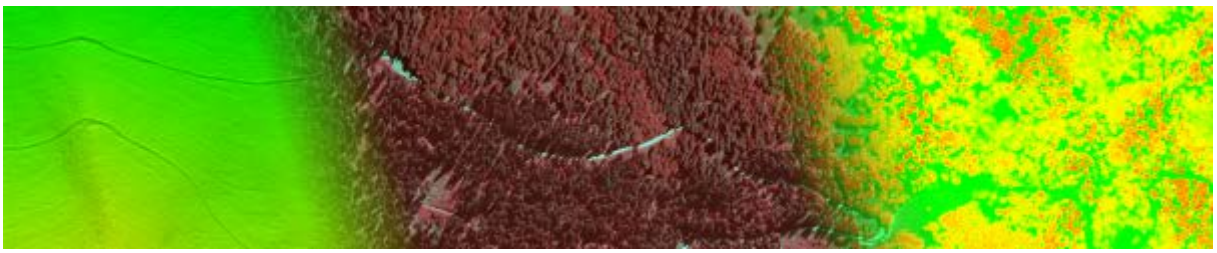

The consortium of the project Interreg Alpine Space NEWFOR

This project has been, co-funded by the European Regional Development Funds, and achieved under the third call of the European Territorial Cooperation Alpine Space Programme 2007-2013.

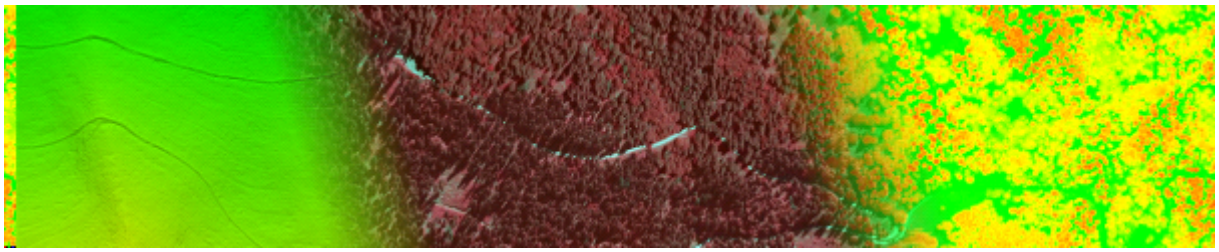

Contents

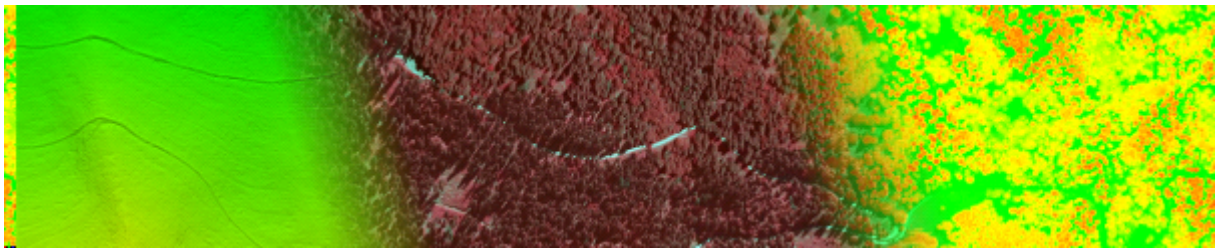

1 Introduction

The geometry of a real surface can be very complex and diverse. It also makes the modeling of a physical process more difficult since different surface features have different effects. Therefore, it is very important to quantify those surface characteristics properly. Diversity of the surface characteristics is also known as *surface roughness* and parameters which should describe it are called *surface roughness indices*. They are introduced in order to improve or simplify modeling of a physical process.

Hoffman and Krotkov (1989) noted that a set of indices should be used for a roughness description instead of a single index because the diversity of surface features is much higher than the capacity of one roughness index to characterize them. However, for some applications, it was reported (Verhoest et al. 2008) that in past years there was a tendency to characterize surface roughness by using just one of the most popular indices like ACF, standard deviation or correlation length. This is our motivation to investigate the relation of roughness indices to particular surface features and to broaden the understanding of surface roughness.

In this report we offer an interpretation of the common roughness indices using several facade samples, all of them manifested with different roughness and surface features. The study also examines:

- cases when it is appropriate to employ a particular index,
- the index ability either to characterize prominent features or to generally describe surface complexity,
- the influence of several processing operators like resampling, detrending and smoothing, and
- the index transition over several scales.

The report is organized as follows: Section 2 discusses characteristics which are beneficial for roughness indices. Then, within the same section, the most common roughness indices are reviewed and then classified. In Section 4 a data set for index testing is introduced. Moreover, the section includes: (a) the description of the instrument used for data aquisition, and (b)applied preprocessing steps. Results are summarized in Section 5.

2 Surface roughness

The section introduces aspects of surface roughness and relates them to applications. Based on these aspects, roughness indices will be later discussed and classifed.

2.1 Roughness analysis

Although the understanding of roughness is diverse over the listed disciplines, there are some important tasks which are common for almost any roughness analysis. Firstly, it is important to define minimum roughness. This is the minimum component of roughness significant for

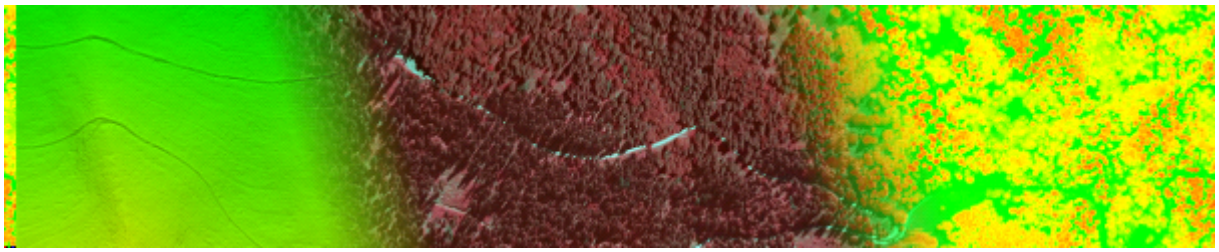

an accurate process description. In the runoff modeling and road roughness, for example, the minimum roughness may be at cm to mm scale, while in the backscatter modeling it may be at cm to dm scale. Moreover, the minimum roughness rules the choice of a measurement instrument, since the sampling interval of an instrument has to be at least two times smaller than the size of the minimum roughness feature (the Sampling Theorem). Second important task is to define estimating unit for roughness analysis. This gives a basis for both spatial analysis and mapping of surface roughness. The results of the later are digital roughness models (DRM) which can be used as inputs in numerical models, e.g. runoff models. The resolution of the DRM, i.e. the size of the estimating unit, primarily depends upon the sampling interval and, usually, the smaller is the better. Next important task is detrending. This procedure should separate the topography component described by the numerical model from roughness. In most cases, models consider just local slope, thus a simple linear detrending is usually enough. Finally, the last task is to define appropriate roughness measure to characterize roughness within the estimating unit. Depending on the complexity of the roughness, this measure can be a combination of roughness indices of just one index.

New technologies for data acquisition have significantly improved the resolution of DRMs. Surface roughness can be now analyzed at resolutions of 1-3m by point clouds derived from terrestrial laser scanning, airborne laser scanning and image matching. However, in some applications, this DRM resolution is significantly higher than an area at which surface roughness has to be modeled. In theoretical backscatter models, for example, this area is equal to the resolution of a synthetic aperture radar (SAR) image, typically 50-100m, while in runoff modeling, roughness should be described for a whole catchment or sub-catchment. At these areas, roughness may be highly heterogeneous, containing sub-regions of different roughness states. These roughness domains have to be identified and delineated, which should be treated as a separate task in roughness analysis.

In some applications, like runoff modeling, the identification and delineation is enough, while in applications like backscatter modeling, it should be followed by a special characterization of the roughness heterogeneity. For example, a pixel of a SAR image may relate to an area that consists of two tillage stats, e.g. plowed and harrowed fields. They carry quite distinctive roughness patterns and will influence the backscatter signal differently. Therefore, roughness for that pixel should be described differently than for pixels associated with a homogeneous roughness state. In the runoff modeling, however, it will be enough just to delineate the two roughness states and to assign appropriate hydraulic resistance value to each, e.g. Manning's values.

2.2 Roughness dimensions

High resolution DRMs certainly provides a big advantage in roughness analysis. But, it is also important to understand some properties of surface roughness to that end. These properties help in describing different types of roughness, and therefore, will be called dimensions here. The roughness dimensions pertain to roughness of an area which is, in our case, the spatial unit at which roughness has to be described, e.g. the resolution of a SAR image or the size of a

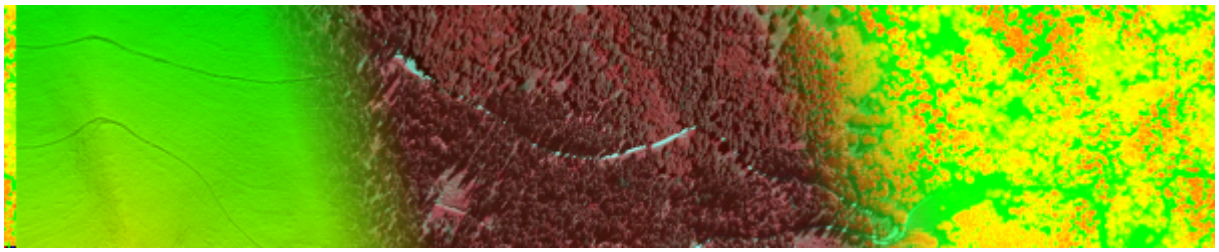

catchment.

2.2.1 Stationarity

Roughness that has the same characteristics at each location of an area is considered to be stationary in this area. Within the area of stationary roughness, a roughness index will always have the same value. However, this is usually not possible in praxis, thus the index values are rather randomly distributed around a value. It should be noted that this property depends upon the measure, i.e. a roughness index, and therefore, roughness can be sometimes stationary or non-stationary, depending upon the used roughness index. For instance, a random noise roughness is stationary in terms of central-moment indices like standard deviation, skewness or kurtosis, while in terms of peak to valley height it may not be.

Roughness stationarity also depends on both estimating unit and presence of trend or any other systematic in the data. The later can be incorporated in index definition, thus some indices are more robust in identifying stationarity than others. The estimating unit, on the other hand, is a parameter in index estimation, and its change leads to different index values. If there is an estimating unit for a roughness index that provides always the same index value, then this estimating unit and index value are intrinsic properties of that roughness. The size of such estimation unit is the characteristic scale of this roughness pattern. Take, for instance, a sine function and the peak to valley height index. The index values will always be different for estimating units less than a period of sine wave, while only for one equal to the period, all the index values will be the same and correspond to the amplitude of that sine wave. Thus, this estimating unit (the period) and this index value (the magnitude) are the intrinsic properties of the observed wave. In addition, the period is the characteristic scale of the roughness pattern given by the sine wave.

Heterogeneous roughness, introduced in the previous section, is an example of Non-stationary roughness. For this type of roughness, index values alter all over the area, but its distribution is not random. The values are rater systematically sub-clustered, indicating the presence of separate roughness domains, i.e. subareas with different roughness pattern. Non-stationarity may come from a process which interrupts the stationarity. An example for this is a pebble orientation in steep slope streams. There, in the middle flow path, the particles are down-stream oriented, whereas on the river banks, they are oriented randomly.

2.2.2 Isotropy

Within an area of isotropic roughness, the index value is independent on an analysis direction. There is no special index targeting isotropy detection, but it is always possible to calculate indices along several differently oriented profiles and use those information to describe the isotropy. In praxis, the index values will never be the same and based on its dispersion, the roughness can be considered either as isotropic or anisotropic. An example of anisotropic roughness are plowed fields, where roughness significantly differ in directions along and perpendicular to the plowed rows. Similarly to the stationarity, the isotropy depends on the length at which is estimated and

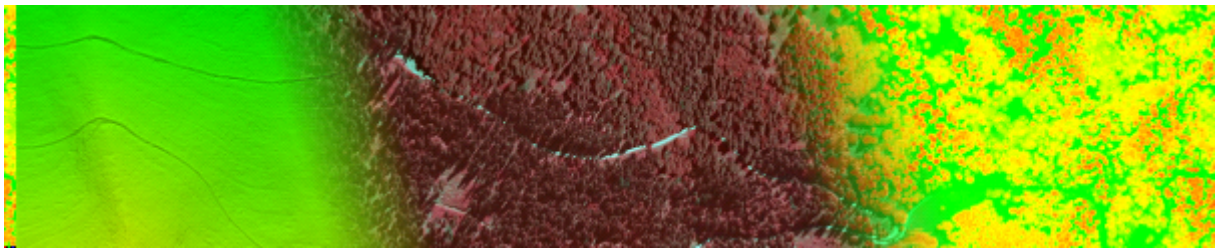

the trend, but it also has an extra parameter - azimuth of the estimating direction. If there is a direction that provides the same index value for all locations within the area, then this direction and this index value are intrinsic properties of that roughness pattern. For a plowed field and the peak to valley height index, it will be the azimuth of the line perpendicular to the plowed rows and the ridge-furrow height, respectively. The estimating length and the trend follow the discussion given for the stationarity, but now it is restricted only to a particular direction.

2.2.3 Scaliness

Scaliness is used to describe roughness which heights fluctuate over several magnitudes. This range of roughness component is only analyzed within the characteristic scale of the roughness pattern. Therefore, scaleness takes into consideration both estimation size/length and trend, i.e. the common parameters for the two previous roughness dimensions. An example for scaliness is a roughness of river beds. The scales in this pattern come from different particles (gravel, pebble, bolder, etc.) that accumulate over the river bed in time. Also, different geomorphological processes may create this type of roughness by interacting with surface over different scales. (Ask BS for an example!). The opposite of scaliness is single-scale and scaleless roughness which heights fluctuate over one or few magnitudes, respectively. An example of this roughness is harrowed filed. The scales can be easily analyzed by magnitudes obtained form the Fourier Transform of the roughness pattern.

2.3 Properties of roughness indices

The resolution of DRMs is the prime unit for roughness characterization. Within this spatial unit, a roughness index should describe particular feature of a roughness pattern. Beside doing this, roughens indices have other properties which may make them more suitable in specific applications. These properties may also serve as a basis for index categorization. Here, the index properties will be identified and described in more detail.

2.3.1 Geometrical meaning

Roughness indices use geometric information of a surface (x, y and z coordinates) to describe surface roughness. As such, they always have a geometrical meaning which depends upon the way how the information is explored. Some indices employ statistics to describe roughness. These indices have gained large popularity over many disciplines, mainly because of their calculation simplicity and a common perception that roughness is natively related to height variation (Linden and Van Doren 1986). Some of the most popular indices from this group are root mean square height (RMSh), standard deviation (Std), average slope and skewness. However, the statistical indices are highly influenced by factors like assumed distribution function, sampling interval and evaluation length, which may be a drawback in some applications (Linden and Van Doren 1986).

Another group of indices is feature oriented. They not only use roughness features like local minima/maxima, but also may use geometric features to describe roughness. A typical

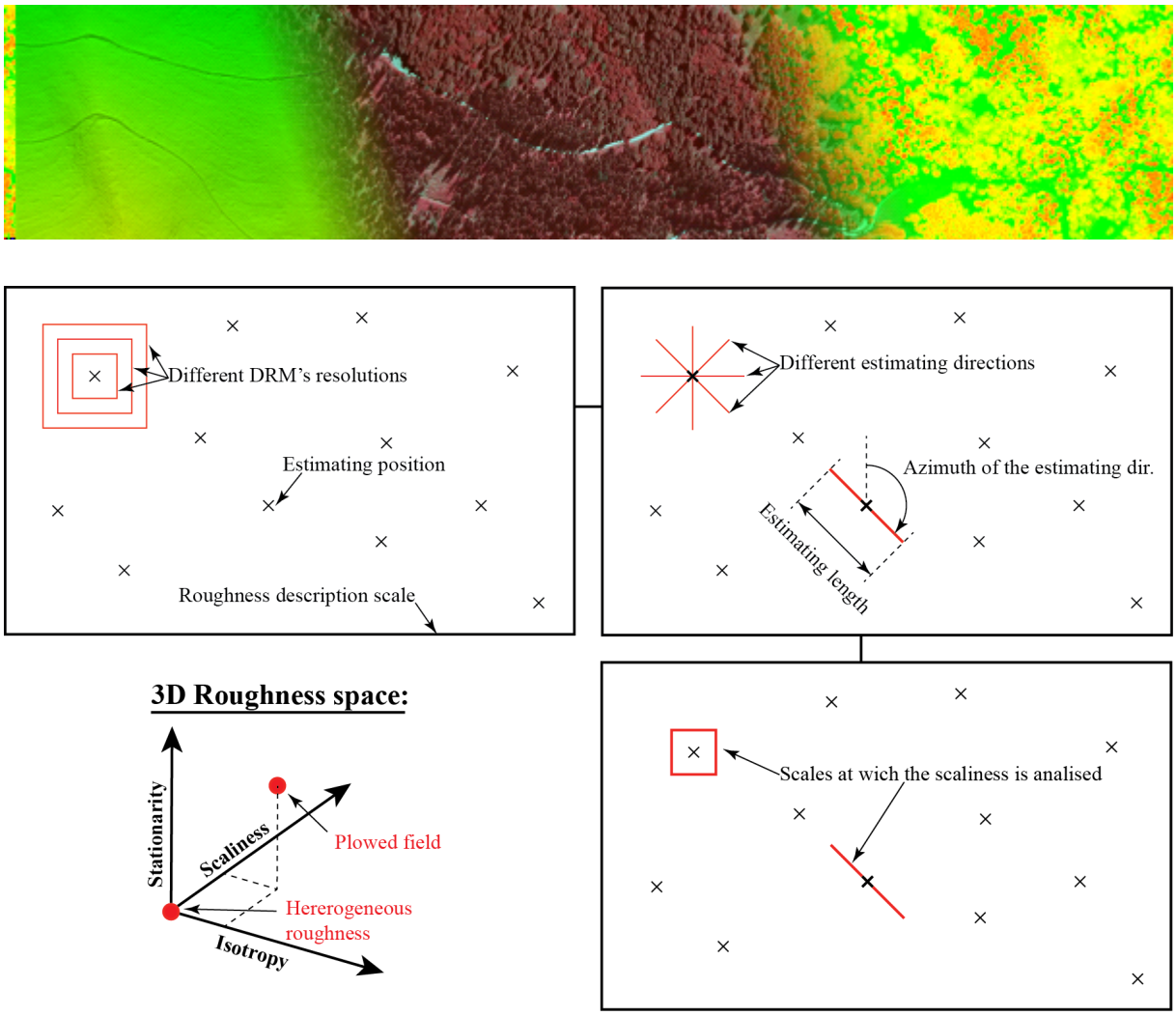

Figure 1: Stationarity, Isotropy and scaliness - the 3D Roughness concept

index of the later is openness which estimates the maximum possible cone constrained by local topography. Examples for the former are indices like local peak height and peak to valley distance/height. There is also a third group of indices that combines both statistics and features. Indices from this group are average peak height or peak frequency.

2.3.2 Physical meaning

It is very important for a roughness index to have a physical meaning, i.e. to be related with surface features important for a physical process. This may ensure index popularity and wide usage in a particular field. Physical meaning of an index is strictly related to a physical process, and the index may either have it or not. In the river-bed roughness, for example, the skewness with positive values indicates the aggregation of fine-particle materials over the coarse-particle river bed (Smart et al. (2004) and Nikora et al. (1998)).

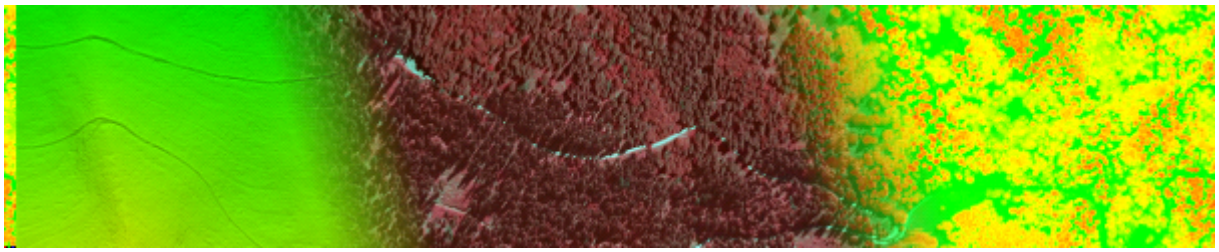

2.3.3 Geometry type

This index property depends on the type of the geometric information included in the index definition. Indices can be categorized in three groups by this property. First group uses only planar information (x and y coordinates). An example is the peak to valley distance index. Second group uses only surface heights, i.e. the z coordinate. Standard deviation and RMSh belong to that group. Finally, third group combines planar and vertical information, and typical indexes of that group are average slope, openness and tortuousity.

2.3.4 Trend awareness

Roughness indices either include information about trend into their definitions or not. In the later case, i.e. when the trend is not included, the index values differ from each other when they are calculated before and after detrending of the data. This, for example, may affect stationarity analysis, where presence of trend may significantly hamper its detection. Therefore, indices that include trend, e.g. standard deviation or tortuousity, are more robust in stationarity detection than indices like RMSh or peak-to-valley height which neglect the trend.

2.3.5 Frequency information

Using the Fourier Transform, roughness can be also represented in frequency domain by the magnitudes and phases of the trigonometric basis. These frequency coefficients carry different type of roughness information and therefore it is important to know which part of the frequency is present in particular index. For example, the autocorrelation function includes only the magnitudes into its definition which in some applications like backscatter modeling is not enough to uniquely describe roughness (cite our previous paper!). Since there are two types of frequency information, i.e. magnitudes and phases, roughness indices may contain either just one of these two or both.

2.3.6 Estimation complexity

Each roughness state has a characteristic value of a roughness index, i.e. the theoretical value. However, this number is not a priory known and has to be estimated. The estimation depends on several factors, which makes the procedure more complicated for some indices than for the others. The factors may come from selected measurement technique, measurement conditions or the estimation procedure itself. The correlation length, for example, requires much stronger measurement conditions and estimating procedure than the RMSh (cite papers from the backscatter modeling!!!). In these studies, the correlation length is found to be highly sensitive on factors like size of the measuring area, sampling interval and number of measurements which just partly define the mentioned measurement conditions. In addition, this index can not be explicitly estimated from the surface heights because a theoretical autocorrelation function has to be estimated first. All these make the correlation length highly difficult to estimate comparing to other indices.

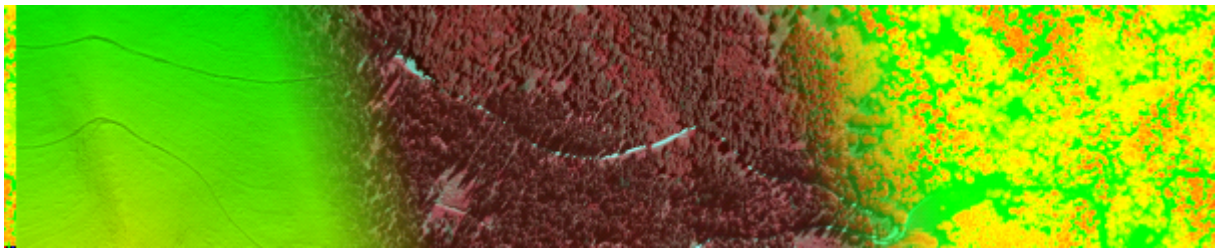

2.3.7 Convergence

One of the most important factors in estimating the index value is size (length) of the estimating area (profile), and therefore, it is treated independently here. Within a homogeneous roughness state, index values should demonstrate convergent behavior while the size of the estimating area is growing. This means that there should be a size after which the index value does not change significantly any more. This size is also called evaluation length (Whitehouse (2003)), and the smaller it is the better. For a particular roughness state, each roughness index has its own evaluation length, which determines their suitability for roughness analysis. (Taconet and Ciarletti (2007) showed that) An estimation of a index at scales less than its evaluation size may lead to its under- or over-estimation.

2.3.8 Derivation order

Sometimes, local statistics of an index may catch the roughness pattern fair better than the index itself. The local variability of the openness index, for example, is found to be much more useful in describing roughness of areas along a watercourse (cite our paper from MODSIM2011!!!) On the other hand, indices may be combined with each other into new roughness measures. An example for that is the effective slope index, defined as the ratio between the RMSh and the correlation length, which is employed in the backscatter modeling to reduce the number of unknowns in the models. Both types of roughness measures are derived from the original indices, either by combining them or by exploring its statistical properties, and therefore, will be treated as index derivatives.

3 Roughness index overview

Roughness features are highly diverse in the nature, which provides a large number of the indices available for its caricaturisation. Here, the focus will be only on the most common roughness indices. The overview balances between indices which gained certain popularity in a particular field and indices that have prominent properties that was discussed in the previous section. For each index, the overview includes its definition, main characteristics as well as links to other indices. The focus will also be on roughness features and applications where the index can be successfully applied.

3.1 Standard deviation (σ)

Standard deviation is a well accepted statistical measure for a surface roughness description. It quantifies surface height variability towards to a predefined trend, and generally, it can be defined as

$$\sigma = \sqrt{\frac{1}{N}\sum_{i=1}^{N}(h_i - T(h_i))^2} \quad , \tag{1}$$

where

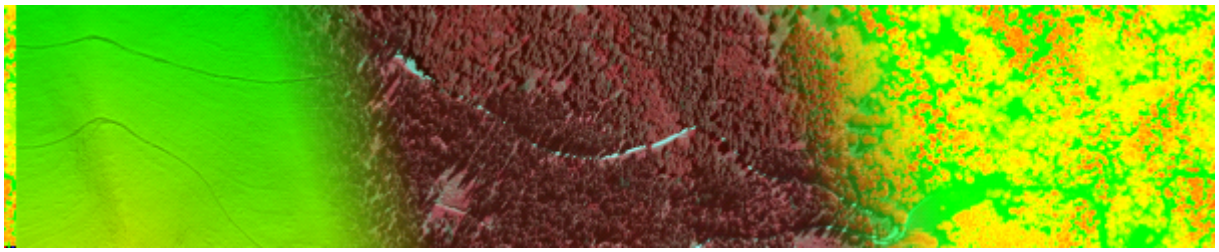

$h_i = h(x_i, y_i)$	...	a surface height
$T(h_i)$	...	a predefined trend
N	...	number of measurements

In the classical case the predefined trend is equal to the average value of surface heights. A regression plane can be also used as a trend description and in this case Eq.(1) calculates the $RMSh$ of surface residuals. With this trend the slope effects in surface heights will be also canceled out.

Darboux et al. (2002) uses the standard deviation of heights, estimated on profiles with the length equal to the correlation length, to characterize soil roughness during a runoff process. They detect a linear dependence between the standard deviation and the storage capacity of the topography. The standard deviation is also used to express river bed roughness, treating it as a random field of elevations in contrast to a traditional approach which is focused on a particle size characterization (Smart et al. 2004, Nikora et al. 1998, Kohoutek and Nitsche 2010). However, they also state that the index is not appropriate for steep mountain streams due to large irregularities in bedforms, present slopes and wide grain size distribution. So, an interrupted stationarity of the surface geometry is hard to explain by this index. Finally, Hollaus et al. (2011) estimated the relation between surface roughness and the width of a backscattered airborne laser saning (ALS) pulse. They used the standard deviation of plane fitting residuals to quantify surface roughness.

3.2 Root mean square height ($RMSh$)

This index is very similar to the standard deviation and they both are popular statistical measures. The main difference is that the standard deviation treats the trend of data as a horizontal line fitted through surface heights while the $RMSh$ dose not take the trend of data into consideration. This actually means that the $RMSh$ estimates an absolute magnitude of height variation and the standard deviation can be seen as a relative measure of it, independent on a height level of variation. As we state in the previous subsection, the $RMSh$ is a special case of the standard deviation with the specific detrending (horizontal plane $z = 0$ is taken as a trend). Therefore, similar surface features can be characterized by using either the $RMSh$ or the standard deviation. The formula for calculating the $RMSh$ is given as:

$$RMSh = \sqrt{\frac{1}{N}\sum_{i=1}^{N} h_i^2} \quad , \tag{2}$$

It can be shown that the $RMSh$ index is a parametrization of the autocorrelation function, when the lag value is set to zero, i.e. $ACF(l = 0)$. In Section 3.4 this will be expressed by an equation.

The $RMSh$ of surface residuals is highly used as a surface roughness descriptor in modeling radar backscattering signals (Verhoest et al. 2008, Lievens et al. 2009, Bryant et al. 2007, Perez-Gutierrez et al. 2007, Davidson et al. 2000). Detrending of original surface heights is the

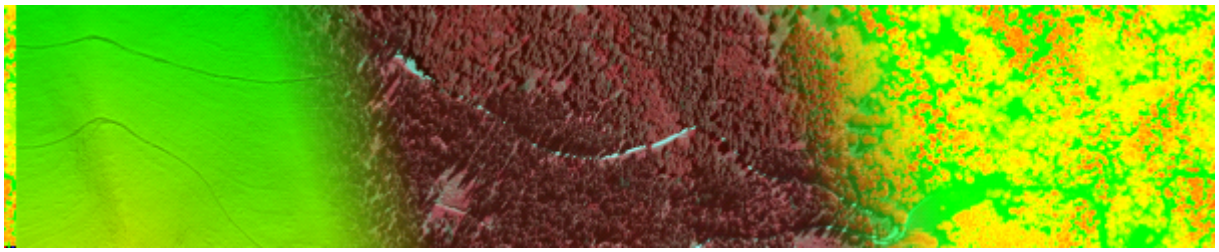

first step in estimating roughness for this application. However, it is assumed that a part of the trend remains in data and the $RMSh$ is seen here as an appropriate index to quantify it.

3.3 Skewness (S_k)

Skewness is a measure which describes a degree of asymmetry from the normal distribution of surface heights. The index can be calculated by:

$$S_k = \frac{\frac{1}{N}\sum_1^N (h_i - \overline{h})^3}{(\frac{1}{N}\sum_1^N (h_i - \overline{h})^2)^{3/2}} \quad , \tag{3}$$

This parameter is using very often in a combination with the standard deviation or other indices that assume the normal distribution of surface heights. Smart et al. (2004) and Nikora et al. (1998) reported a positive skewness for river bed elevations. They relate it with fine scale sediment transport which causes a reduction of deviation in elevations below the mean bed level. Additionally, it is noted that the detected skewness is in contrast with the skewness of a grain-size distribution.

3.4 Autocorrelation function (ACF)

This function is highly related to the spatial statistic measure called *Variogram* $\gamma(l_i)$, where l represents a horizontal lag value. Both functions carry the same information about a surface but differently expressed. Variograms quantize variation, while the ACF estimates a degree of similarity for surface heights. It is irrelevant which one is used and discussion below, is valid for both functions. Formulas for calculating the ACF and the variogram at a lag value l_j are:

$$ACF(l_j) = \frac{1}{N}\sum_{i=0}^{N-1} z(x_i)z(x_i + l_j) \tag{4a}$$

$$\gamma(l_j) = \frac{1}{2}\frac{1}{N}\sum_{i=0}^{N-1} (z(x_i) - z(x_i + l_j))^2 \tag{4b}$$

As we can see, absolute heights are involved in both definitions and therefore, the slope effects should be removed before any calculation.

Next equations offer a relation between the mentioned functions and additionally with the $RMSh$ index.

$$\gamma(l_j) = ACF(0) - ACF(l_j) = (RMSh)^2 - ACF(l_j) \quad , \; l_j = j * \Delta l \tag{5a}$$

$$ACF(0) = \frac{1}{N}\sum_{i=0}^{N-1} z(x_i)z(x_i) = (RMSh)^2 \tag{5b}$$

where j ($j = 0, 1, 2, \ldots$) controls the total number of estimated lags, while Δl represents a horizontal increment.

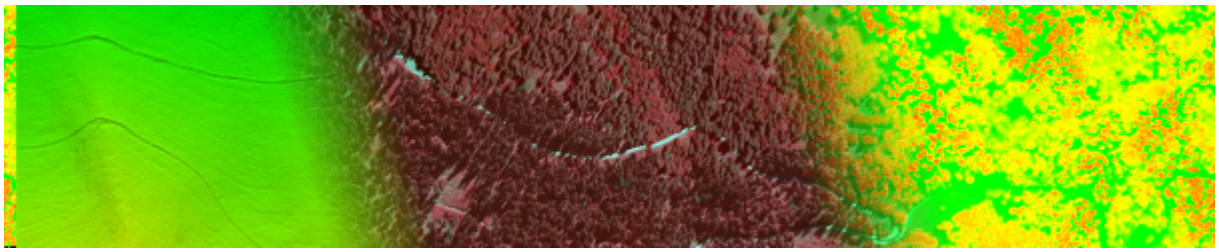

Darboux et al. (2002) use the variogram to estimate changes at different scales in soil roughness during a rainfall event. Due tu a rainfall simulation a starting surface structure was modified in a heterogeneous way, changing also conditions for a runoff generation. However, those new features in the surface were not possible to be detected by the variogram analysis performed in their experiment. Taconet and Ciarletti (2007) quantified row periodicity of a ploughed soil by using a directional ACF. The function is also highly used to describe general target geometry which appears as one of the key parameters in the interpretation of backscattered radar signals (Verhoest et al. 2008, Lievens et al. 2009, Bryant et al. 2007, Davidson et al. 2000). Finally, Nikora et al. (1998) applied a so called *structure function* $D(\Delta x, \Delta y)$ to quantize the isotropy of river bed roughness. The last parameter is equivalent to the variogram function.

3.5 Correlation length (l_{cor})

This index is a parametrization of the ACF and represents a distance for which the ACF falls below $1/e$ of its zero lag value (Taconet and Ciarletti 2007):

$$ACF(l_{cor}) = ACF(0) \cdot (1/e) = (RMSh)^2 \cdot (1/e) \implies l_{cor} \ . \tag{6}$$

From the last equation we can conclude that the $RMSh$ and the correlation length can not be treated as independent variables. However, the equation also converts vertical roughness information (the $RMSh$) to a horizontal one (the correlation length) which is recognized as an interesting surface feature in many applications.

Kohoutek and Nitsche (2010) and Smart et al. (2004) are used this index for a stream bed morphology characterization. It was noticed from Smart et al. (2004) that the directional (transferal and longitudinal) correlation lengths was not able to detect subtle river bad differences along the stream-wise and cross-flow directions. Nikora et al. (1998) tried to relate a so called *linear scale* value to a bed particle axial size but they find no significant correlation between them. However, they suggest using the index for quantifying a horizontal length of river bed roughness. The linear scale index is a parametrization of the mentioned structure function and can be seen as an equivalent to the correlation length. Correlation length is especially popular in the soil roughness characterization for modeling of backscattered radar signals. All the studies about this application, listed in Section 3.4 , take into consideration the correlation length, as well. Evaluation length, number of evaluation sites, detrending procedure, horizontal and vertical accuracy and sampling frequency are recognized as factors influencing an estimation of the index. This topic has been treated intensively in Lievens et al. (2009), Verhoest et al. (2008), Taconet and Ciarletti (2007) and Bryant et al. (2007).

3.6 Tortuousity (T_B)

This index is firstly introduced by Boiffin (1984), and represents a ratio between the real length of a profile (L) and the length of a straight line parallel to the average slope of the profile (L_0):

$$T_B = \frac{L}{L_0} \ , \tag{7}$$

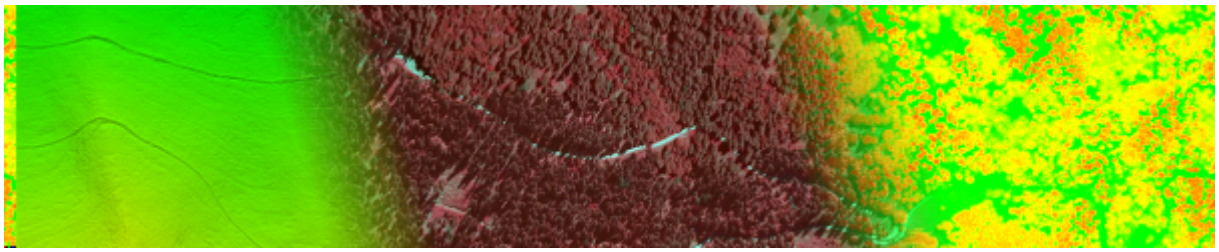

At the beginning a chain method was used for its measurement, while nowadays, the index can be easily extracted from surface heights collected by any instrument. Consequently, the given definition is later extended in order to take into consideration three-dimensional data (Hobson 1972, Helming et al. 1993). This index is considered now as a ratio between the real surface area (A) and the area of a plane parallel to the average slope (A_0). It should be noted that the given definitions cancels the slope effect. However, the index strongly depends on a sampling frequency and therefore it is not appropriate for a comparison between roughnesses of different magnitudes (Kamphorst et al. 2000).

Taconet and Ciarletti (2007) demonstrate that the index is able to detect soil roughness changes due to a simulated rainfall event. Additionally, they noted that different rates of roughness degradation over ridges and "interrows" areas can be well distinguished by this index, too.

3.7 Peak to valley height (PVh)

This index is used in surface metrology where surface roughness is considered as irregularities coming from a manufacturing process (Whitehouse 2003). A Peak to valley height is a feature oriented index but it can also be seen as a statistical measure which takes the two most extreme heights of a surface. This index can be calculated by the next formula:

$$PVh = h_{max} - h_{min} \ , \tag{8}$$

where the h_{max} and the h_{min} are the maximum and the minimum height of estimated surface, respectively. Any slope effects should be removed from surface heights before calculation of the index.

There are also several other feature oriented indices like peak to valley horizontal distance (PVd), average peak to valley height, average peaks/valleys height, peak frequency, etc. However, those indices will not be specially analyzed here.

Table 1: Overview of the common roughness index and its properties as defined in Sec. 2.3

	Geom. meaning	Geom. type	Trend aw.	Freq. info	Est. complex.	Deriv. order
Standard Deviation	Yes - Stat.	Heights	Yes	Mag.	Low	0
RMSh	Yes - Stat.	Heights	No	Mag.	Low	1
Skewness	Yes - Stat.	Heights	Yes	Mag.?	Low	0
Autocorrelation Function	Yes - Stat.	Both	No	Mag.	Medium	0
Correlation Length	Yes - Stat.	Both	No	Mag.	High	1
Tortuousity	Yes - Feat.	Both	Yes	Both?	Medium	0
Peak-to-valley Height	Yes - Feat.	Heights	No	Both?	Low	0
Openness	Yes - Feat.	Both	No	Both?	Medium	0

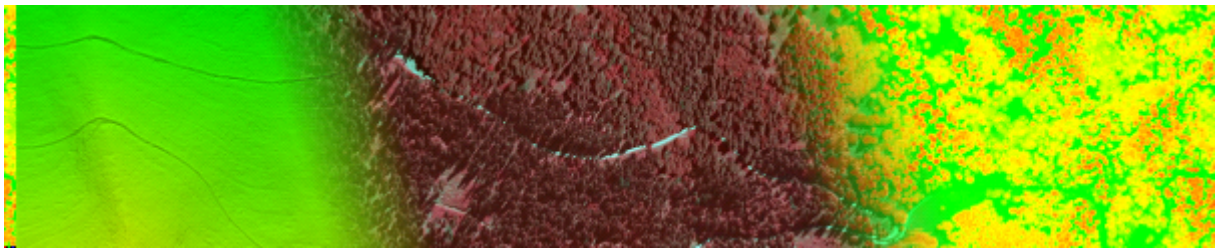

4 Data

Six facade samples shaped by different techniques and particle sizes are analyzed in this report. Each of them has a distinctive roughness pattern which was scanned and represented by a corresponding point cloud. We will firstly describe the instrument which is used for the data acquisition. Then we will describe processing steps which are done in order to create DSMs and finally we will discus interesting roughness features present in the facade DSMs.

4.1 Measurement device

The *METRIS MCA 3600 M7* (Manual Coordinate measuring Arm) is used for data acquisition. This is a precise geometrical measuring system specified for 3D coordinates collection from a relatively small objects (up to 2 m). The instrument can operate in three different acquisition modes: hard probe, continuous scanning and laser scanning. The last one allows fast object scanning with a triangulation laser scanner mounted on the head of the arm, which was suitable in our case. Any movement of the head is recorded in the arm relative coordinate system resulting to locally referenced scans of the object. The final product of this instrument is a point cloud of the observed object.

Triangulation laser scanners (TLS) are actually active 3D scanners which combine laser and digital camera senors to reconstruct the distance between a object point and the sensor. The TLS mounted on the arm emits a set of oriented laser rays in the visible domain (red, 640 nm), forming a stripe pattern of laser light over the estimated object. The emitted laser rays are placed in a plane and the stripe pattern on the object represents the intersection of those two bodies. Accordingly, the digital camera capture the pattern allowing the reconstruction of directions from reflected rays. Subsequently, known distance between the laser emitter and the digital camera as well as known direction of the emitted ray together with reconstructed direction of the reflected ray allow to calculate a distance between the sensor and the illuminated stripe segment. Finally, moving the TLS fixed on the arm head it is possible to collect a strip of 3D points over the object.

The explained design is a main reason that a TLS has a characteristic spatial patten of the acquired data. Figure 2 shows this pattern where several horizontally oriented strips are measured over a sub-area of the facade sample M3. There are several pattern features which can be observed in this point cloud. Firstly, the sampling frequencies along and across strip are highly different in the value as well as in the structure. Then, the overlapping areas usually appear with irregular shapes and sizes (feature (iv)). Finally, some repeated scans can be present in data which will interrupt the existing sampling frequency (feature (iii)).

Across strip sampling frequency is more homogeneous and is controlled by a resolution of the digital camera sensor and selected operational strip width (feature (ii)). We decide to use the full sampling potential of the instrument during the data acquisition and restrict the strip width to 50 mm. Additionally, the resolution of the digital camera is 1000 points per each stripe leading to the across sampling frequency of 0.05 mm/stripe.

On the other hand, the along strip sampling frequency is constrained by the way of the TLS

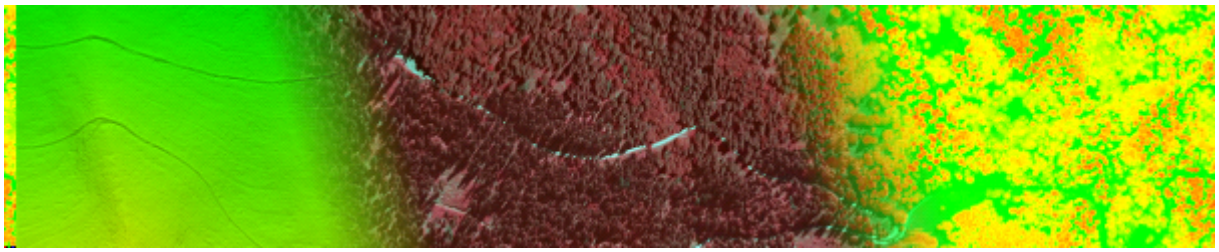

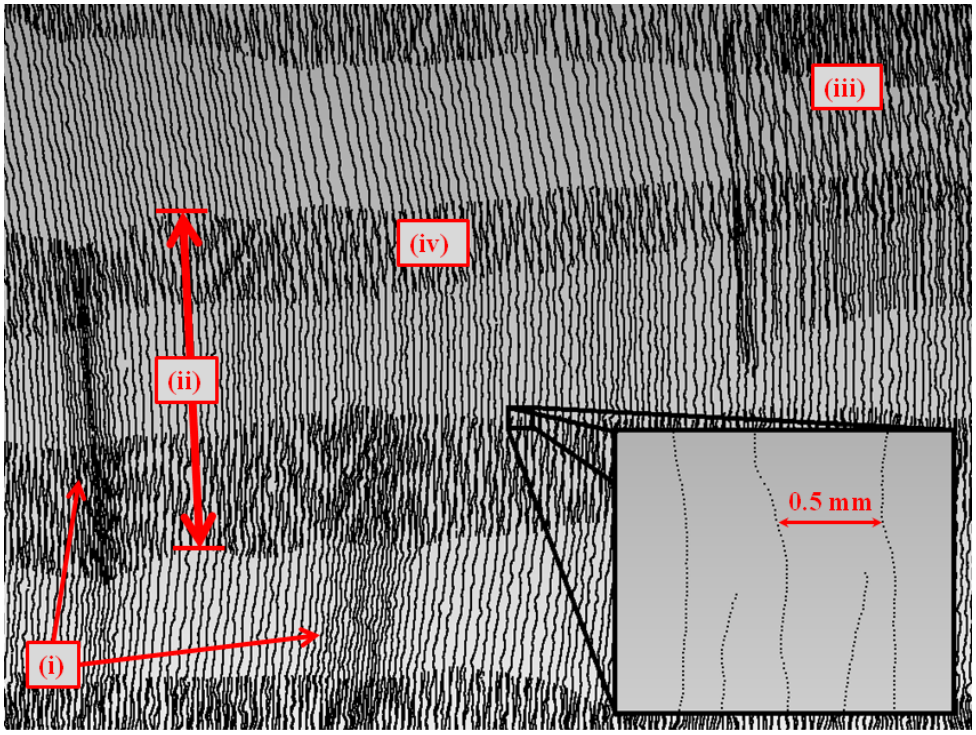

Figure 2: Spatial pattern of the point cloud acquired by the triangulation laser scanner mounted on the arm

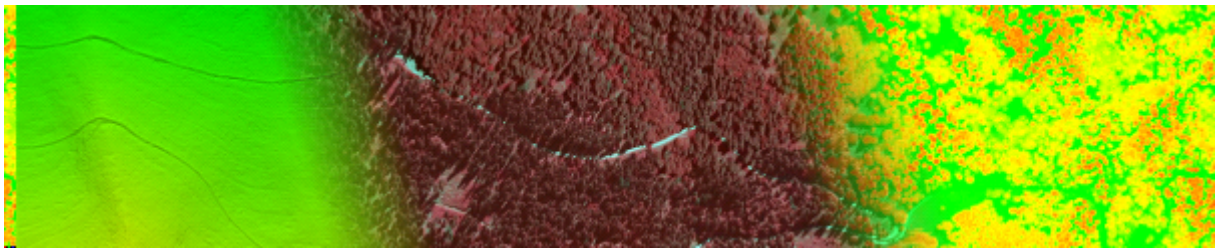

movements over the object. This is done by operator hand movement and as a consequence there are some areas where concentration of stripes is much higher than in other parts (feature (i)). Due to this heterogeneity it was not possible to estimate the exact along strip sampling frequency, however we observed that neighboring stripes are approximately spaced with 0.5 mm.

The explained sampling pattern is highly complex and is very different for all six data sets. In order to avoid any influence of this effect during the index calculation process we decide to create grid digital surface models (DSM) from our original data sets. Those grid DSMs are then used for the visual interpretation and the index calculation.

4.2 Preprocessing

In this subsection we will explain how several series of facade DSMs are created. Those DSMs series are the consequence of performing several processing operations on the starting data sets and should offer a base for discussing index sensitivity to those operations. In order to calculate those DSMs series, the original data are first cut to a sub-area and then different DSMs are calculated.

Sub-area extraction: Each facade sample was scanned by the measurement arm and six point clouds where collected. Due to the high sampling frequency of the arm the point clouds where with a large number of surface points (>10 M). Therefore, we decide to restrict our calculations to an appropriate sub-area. For all six point clouds, those sub-areas where defined as rectangles of the equal sizes, with larger and smaller sides of 181 mm and 114 mm, respectively. The following processing steps are done based on those point clouds.

DSMs generation: Although the sub-areas where of the same size and shape, due to the different sampling patterns the number of points in them was very different, ranging from 550 K to 950 K points. Therefore, the first step in the DSM generation was deducted to remove the heterogeneity in the point distribution. The point clouds corresponding to the six sub-areas are resampled to 0.1 mm regular grids using the moving plane interpolation based on sixteen neighboring points per each grid location. On this way, six ***0.1 mm grid DSMs*** are created representing the facade surfaces (see Figure 4).

The next processing step was introduced in order to create DSMs which will be free of trend. This is done by fitting the orthogonal regression plane through all 0.1 mm grid DSM points and taking the residuals as new heights. Consequently, six ***0.1 mm detrended grid DSMs*** are created for our facade surfaces.

Besides detrending procedure, the 0.1 mm grid DSMs are also resampled to ***0.5 mm grid DSMs*** using the nearest neighboring method. Then, those new DSMs are detrended, again using the orthogonal regression plane residuals. The resulting layers, obtained after two mentioned operations, represent ***0.5 mm detrended grid DSMs*** for the six facade surfaces.

We also were interested to estimate effects of smoothing operator to index values. This was a reason to additionally perform the mean filter with a 7×7 kernel on the 0.5 mm grid DSMs. The resulting smoothed DSMs are then detrended on the same way like in the two previous cases. Finally, six ***0.5 mm smoothed and detrended grid DSMs*** are calculated for the facade samples.

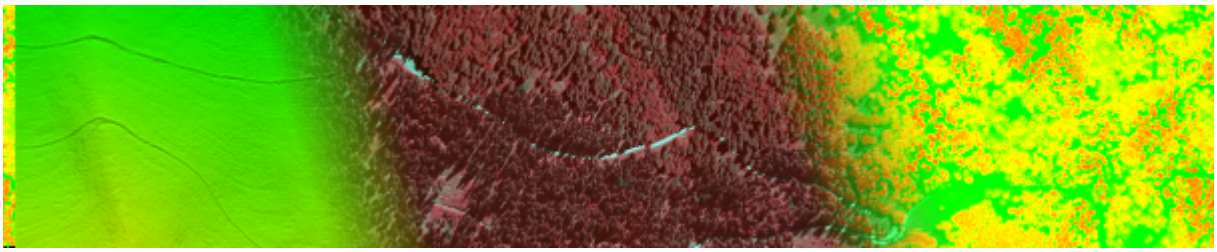

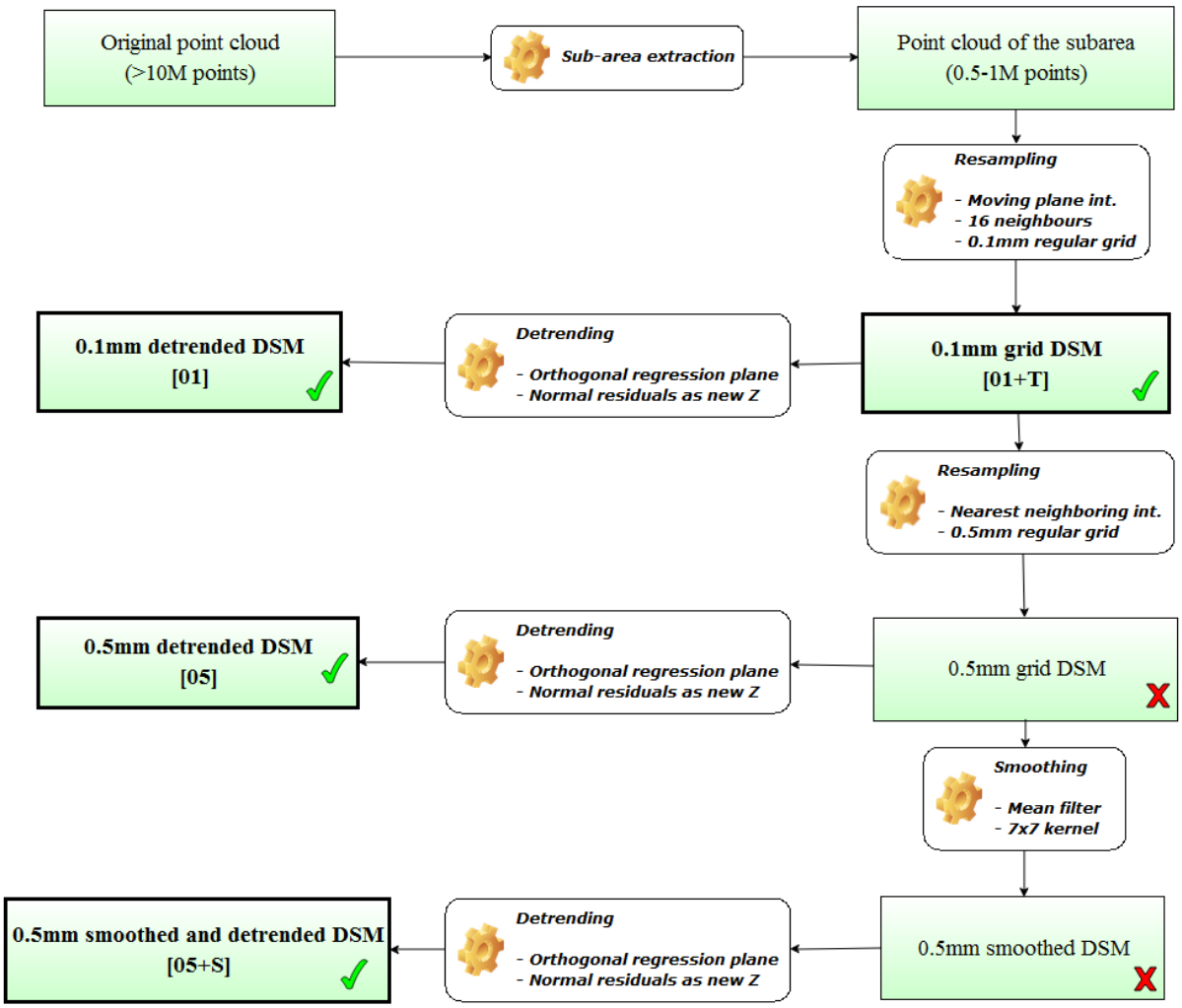

Figure 3: Implemented workflow for the facade DSMs calculation. For each facade point cloud this workflow is performed independently

As it can be seen, several different DSMs series are calculated after performing the explained procedure. However, only four datasets are selected for the index analysis. We will list here those DSMs series and give labels which are used for them:

1. *the 0.1 mm grid DSMs* $\rightarrow [01 + T]$
2. *the 0.1 mm detrended grid DSMs* $\rightarrow [01]$
3. *the 0.5 mm detrended grid DSMs* $\rightarrow [05]$

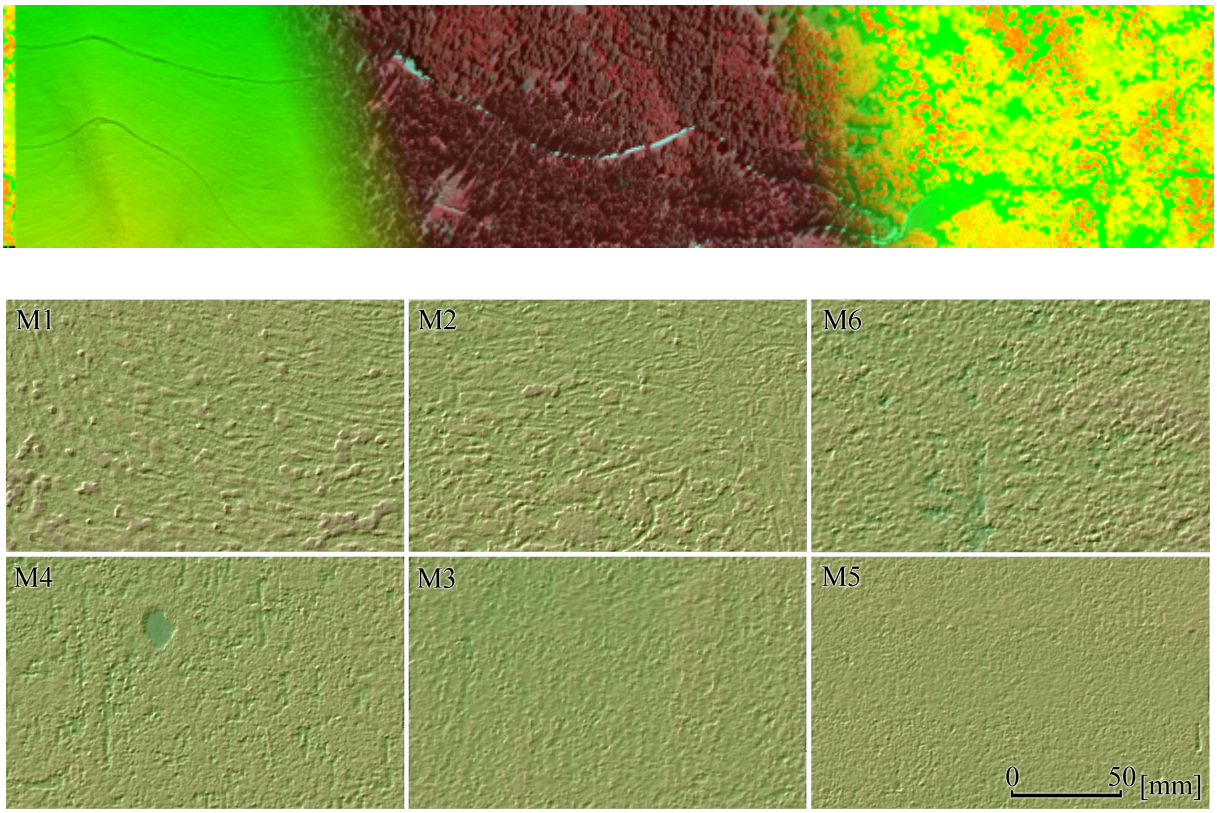

Figure 4: Digital surface models of the facade samples

4. *the 0.5 mm smoothed and detrended grid DSMs* $\rightarrow [05 + S]$

4.3 Description

Before a roughness index assessment it is very important to describe different roughness in our test data set. This can be done only if the understanding of the roughness in the facade samples exist. Therefore, for the purpose of this study, we will assume that the roughness of the facade samples is related to the surface complexity. Additionally, we will assume that this complexity is demonstrated by different magnitudes and frequencies of surface height fluctuation. This means that for sinusoidal surfaces of the same frequency, those with higher amplitudes will be assumed as rougher while, for surfaces of the same amplitude, those with higher frequencies would be rougher. Finally, for surfaces with irregular and regular frequencies, the first ones will be assumed as rougher surfaces. This understanding of roughness is in coordination with Hoffman and Krotkov (1989).

Figure 4 provides an overview for the six DSMs of the facade samples. Roughness presented by those surfaces will be described and ranked with respect to the given understanding. Positions of the given DSMs in the figure are in coordination with decreasing roughness, ranging from left to right in first and second row. DSMs in the first row are with higher magnitudes and lower frequencies of the height fluctuations comparing to ones in the second row. For both rows the degrees of frequency irregularities are ranging from left (high) to right (low).

Facade sample M5: It is one with the lowest amplitude and the highest frequency of height fluctuation among the observed DSMs. They frequency irregularities are very small which, in general, makes that this facade sample is considered as one with the lowest roughness. Surface

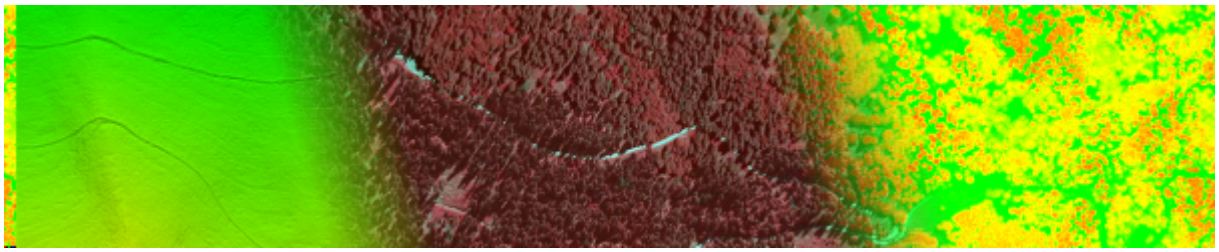

heights are here concentrated around the maximum value and the magnitude deviation seams to be moderate, behaving as holes in an upper layer.

Facade sample M3: For this DSM the hight fluctuation appears with a slightly lower frequency and one order higher magnitude deviation than for the facade M5. On the other side, there is almost no frequency irregularities and the magnitude itself is similar to the previous facade. Finally, surface heights are mainly concentrated around the minimum value, behaving as small hills over a flat topography.

Facade sample M4: Frequency of the height fluctuation as well as the concentration of the heights for this sample are very similar to the facade M5. However, serious interruptions in the frequency can be observed making this facade sample with higher roughness than the facades M5 and M3. Those frequency irregularities cause that the magnitude deviation appears in two separate scales: a moderate (similar with one in the facade M5) and a higher order one which is even higher than deviation in the facade M3. Additionally, moderate magnitude deviations dominate over the scene while the second ones appear just in small sub-areas.

Facade sample M6: This facade sample is very similar to the facade M3, i.e. the frequency of height fluctuation and its irregularities are more or less similar for both. However, the magnitude in this sample is much higher than for all previous samples. In addition, the magnitude dispersion is very high and acts over a single scale. Therefor, this facade sample is considered to have the third biggest roughness among the DSMs.

Facade sample M2: This facade sample represents a very complex surface where the magnitude dispersion performs over three different scales. Due tu this complexity, it is very hard to recognize presence of any frequency in the height fluctuation. The DSM looks like a combination of irregularly shaped hills over a flat topography where the high magnitude dispersion dominate. Because of those irregularities and the very high magnitude, the facade M2 is assumed to have the roughness bigger than the facade M6.

Facade sample M1: Characteristics which are noted for the facade M2 are also valid for this one. The only difference is that the height fluctuation for the facade M1 are additionally systematically oriented, following an arc movement from the upper left corner to the right side of the DSM. This systematic makes the roughness assessment more complex, and therefore, this facade is assumed to have the highest roughness.

5 Results

The results are organized in two subsections. The first subsection is focused on the calculated index values, whilst the second subsection demonstrates the index change over several scales. In both subsections the calculated results for a facade can be based on four different dataset types. Those datasets correspond to the DSMs explained in Section 4.2:

1. the 0.1 mm DSM [01+T],
2. the 0.1 mm detrended DSM [01],
3. the 0.5 mm detrended DSM [05] and

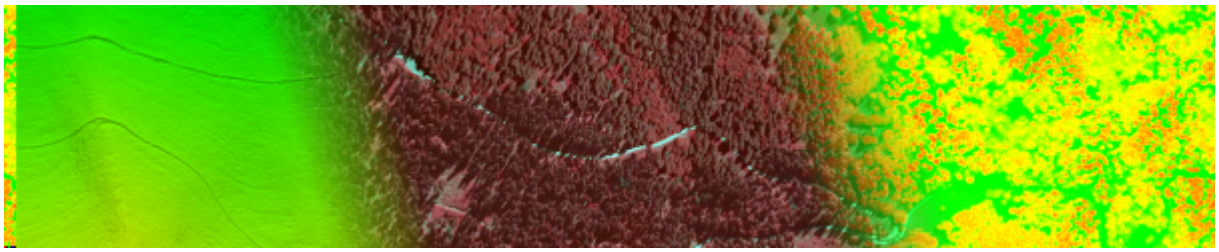

4. the 0.5 mm detrended and smoothed DSM [05+S].

5.1 Indices

The results in this subsection are further divided in several subsections that treat each index independently. The present index values are mainly organized in tables and figures. They should answer how is an index sensitive to different processing operators (detrending, smoothing, etc.) and should offer a base for a facade roughness ranking.

There can be three different types of information present in the tables. The first type is the index values which are listed in separate rows. Each row corresponds to a separate facade sample. The second type is additional columns that are mainly derived from the first type, i.e the index values. The last type of information is statistics calculated for the previous two types.

5.1.1 RMSh and Std

Table 2 summarizes the root mean square height (RMSh) and the standard deviation (Std) values for all six facade samples. Three extra columns are also given, where two of them are named 'Std diff' and one is named 'Nor (Std diff)'. First 'Std diff' represents the difference in the Std of the DSMs with and without trend. Those information should quantify the amount of linear trend present in the starting data sets. Second 'Std diff' is the difference in the Std of the smoothed and non-smoothed DSMs. Sensitivity of the Std index to the smoothing operator should be estimated by those values. The 'Nor (Std diff)' however, takes the starting power of a signal into account and therefore, estimates the sensitivity to the smoothing more objectively.

Facade sample	RMSh [01+T]	Std [01+T]	Std [01]	Std diff [01+T]-[01]	Std [05]	Std [05+S]	Std diff [05]-[05+S]	Nor (Std diff) $\frac{[05]-[05+S]}{[05]}$
M1	99,981	0,381	0,367	0,014	0,366	0,283	0.083	0.227
M2	99,902	0,331	0,299	**0,032**	0,299	0,213	**0.086**	0.288
M3	**99,682**	0,242	0,217	0,025	0,217	0,172	0.045	**0.207**
M4	99,782	0,263	0,250	0,013	0,250	0,181	0.069	0.276
M5	**99,982**	**0,162**	**0,151**	**0,011**	0,152	0,105	**0.047**	**0.309**
M6	99,843	**0,390**	**0,370**	0,020	0,370	0,292	0.078	0.211

Table 2: RMSh and Std overall statistics

In coordination with calculated values we can say that the RMSh values are significantly higher than the Std ones for the datasets where trend is not removed. On the other hand, values for both indices are equal for all detrended data sets.

With respect to the Std values for data with and without a trend, there can be seen a clear reduction of the index for all facade samples. This just prove the assumption from the beginning of this section that the detrending has direct influence on the Std index. However, values in the first 'Std diff' show that absolute linear trends are very low for all the six facade samples. Besides, we can say that facade M2 has the biggest, while facade M5 has the lowest linear trend.

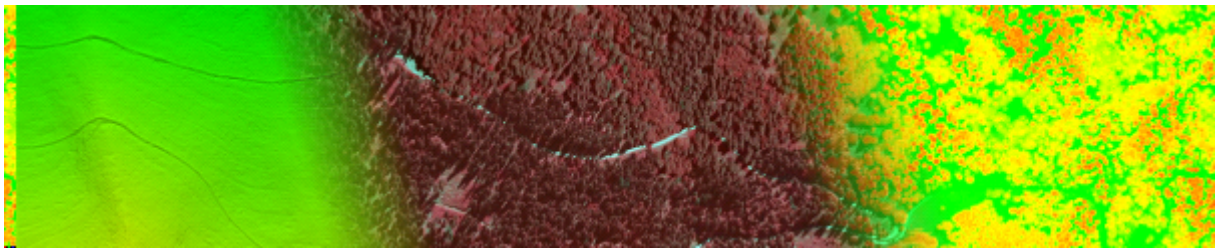

Table 2 also illustrates that grid size dose not influence almost nothing either to the Std or the RMSh index, while both are highly dependent on the smoothing. Facades M2 and M5 show the highest and the lowest Std reduction due to the smoothing, respectively. Still, it is interesting that the facade M5 at the same time demonstrate the highest relative reduction of the Std (Table 2, column 'Nor (Std diff)').

5.1.2 Peak to Vally height (PVh)

A table, similar to previous one, is prepared for this index. There are three different types of information in this table. First are PVh values calculated based on the four facade data sets. Second are the data in the last three columns, representing the difference in PVh values. Those data are calculated in order to estimate the index sensitivity to the detrending, resampling and smoothing operators, respectively. Third are the values placed in the last row. The first four numbers in that row represent standard deviation of the PVh values corresponding to a specific DSM data set. The other three numbers show average of absolute 'PVh diff' for the corresponding column.

Facade sample	PVh [01+T]	PVh [01]	PVh [05]	PVh [05+ S]		PVh diff [01+T]-[01]	PVh diff [01]-[05]	PVh diff [05]-[05+S]
M1	2,851	2,742	2,531	1,934		0,109	**0,211**	0,597
M2	2,239	2,411	2,378	1,773		-0,172	0,033	0,605
M3	2,101	2,243	2,126	1,418		-0,142	0,117	0,708
M4	2,157	2,044	2,001	1,664		0,113	0,043	**0,337**
M5	**1,955**	**1,89**	**1,847**	**1,012**		0,065	0,043	**0,835**
M6	**3,277**	**3,029**	**3,011**	**2,213**		0,248	**0,018**	0,798
	0.518	0.430	0.422	0.418		0.142	0.078	0.647

Table 3: PVh overall statistics

Table 3 shows that the facade M6 has the highest while the facade M5 has the lowest PVh values over all the DSM data sets. Other two facades M1 and M2 also keep their absolute ranking over the data sets while this is not a case for the facades M3 and M4. Furthermore, the facades M3 and M4 are with lower PVh values compared with the facades M1 and M2.

The dispersions of the PVh values decrease permanently, moving from the trend DSM to the smoothed DSM data set; in fact, the biggest drop appears after the detrending while for other operators the decreasing is rather moderate. On the other hand, the transition of the PVh values over the datasets is not straightforward. This is especially because the detrending provides an increase of the PVh value for some facades, i.e. M2 and M3 (see first 'PVh diff' column). Two other operators however, demonstrate the decreasing of the PVh value for all the facades, where the smoothing operator makes a considerable change of the index.

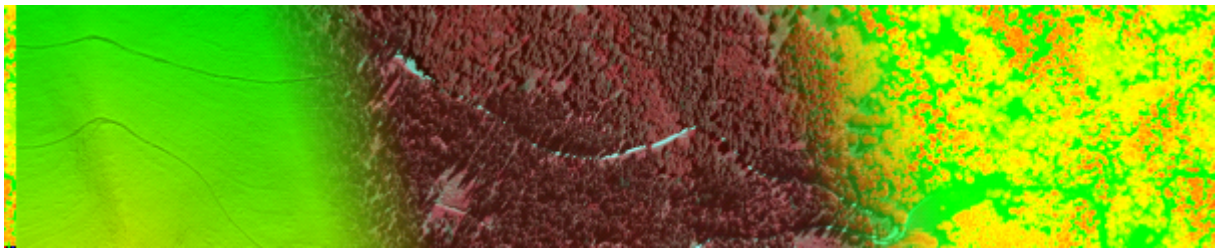

5.1.3 3D distance between peak and valley points (PVd_{3D})

Information carried by this index complement the PVh values since they explain how far apart the extreme points from each other are. We again prepare the table with the index values calculated based on the four data sets (Table 4). The change of the index value, over the operators, is present there and allows to determine if the extreme points remains the same during the data processing.

Facade sample	PVd_{3D} [01+T]	PVd_{3D} [01]	PVd_{3D} [05]	PVd_{3D} [05+ S]
M1	83,045	83,042	47,827	105,166
M2	115,515	91,397	90,553	91,315
M3	46,348	199,601	198,924	109,227
M4	65,753	72,464	65,462	111,508
M5	68,357	108,701	108,432	118,471
M6	134,438	94,624	94,442	112,099

Table 4: PVd_{3D} overall statistics

All the PVd_{3D} values in the Table 4 are different which means that there is no one pair of the extreme points which remains the same during the data processing.

5.1.4 Skewness S_k

The values of this index are summarized in Table 5. The last two columns there, emphasize the difference in the S_k with respect to the detrending and smoothing operators, respectively. The a[1] and b[2] values given in last row, represents statistics from the corresponding columns.

Facade sample	S_k [01+T]	S_k [01]	S_k [05]	S_k [05+ S]		S_k diff [01+T] -[01]	S_k diff [05]-[05+S]
M1	**0,97**	0,767	0,767	0,895		0,203	-0,128
M2	0,666	0,359	0,36	0,485		**0,307**	-0,125
M3	0,076	0,267	0,267	0,375		-0,191	-0,108
M4	-0,869	**-0,918**	-0,917	**-1,275**		0,049	0,358
M5	**-0,055**	-0,053	-0,059	0,307		**-0,002**	**-0,366**
M6	0,249	**-0,016**	-0,015	**0,013**		0,265	**-0,028**
a	0,637	0,567	0,567	0,747	b	0,1695	0,1855

Table 5: S_k overall statistics

[1] $a = \sqrt{\frac{1}{6}\sum_{i=M1}^{M6}(S_k(i) - \bar{S}_k)^2}$
[2] $b = \frac{1}{6}\sum_{i=M1}^{M6}|S_k(i)|$

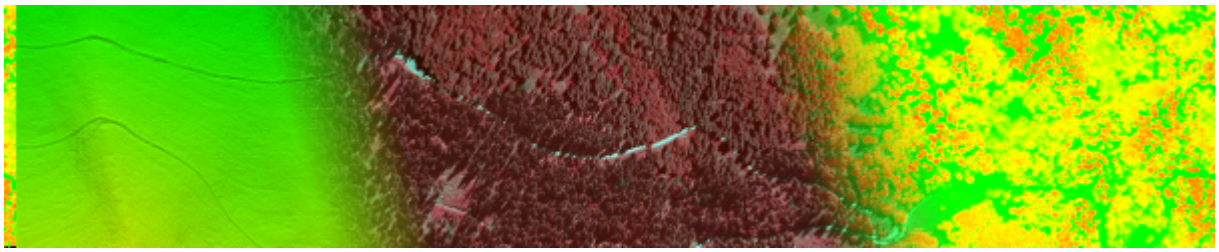

Presented results show that the skewness is very sensitive to the detrending and smoothing operators, while the resampling, on the other hand, hardly provide any change in the index. It should be stressed that the smoothing operator makes extreme deformation of the S_k values for all the facade samples, expect the M6 which data remain non-skewed.

There are four possible patterns of the index change after performing the detrending operator:

1. from a non-skewed to a skewed data
2. from a skewed to a non-skewed data
3. data remain skewed
4. data remain non-skewed

All of those cases are demonstrated by some of the facades in Table 5. The facade M3 is example for the first case while the facades M6, M1 and M5 correspond to other three, respectively.

5.1.5 Autocorrelation function ACF and correlation length

The geostatistical analysis of the facade samples is done based on the calculated global and directional ACFs. We will first present results of the global ACF estimation and then briefly discuss the directional ACF.

The global normalized ACFs are calculated from the corresponding global variograms which where estimated in the software VESPER (Whelan et al. 2002). The formula proposed in Blaes and Defourny (2008) is used for this conversion:

$$\widetilde{ACF}(l_i) = 1 - \frac{\widetilde{\gamma}(l_i)}{\widetilde{\gamma}(\infty)}, \tag{9}$$

where

l_i	...	a horizontal distance, i.e. lag value
$\widetilde{\gamma}$	...	fitted variogram
$\widetilde{ACF}$	...	corresponding ACF fit
$\widetilde{\gamma}(\infty)$	...	the value of the fitted variogram for an infinite distance

We decide to estimate the global variogram under the range of 60mm which corresponds approximately to the half of the smaller side of our estimated area. One group of facade samples (M1, M2 and M4) reached the maximum variation and converge under this range, while the other three samples (M3, M5 and M6) did not. Therefore, the facades are interpreted in two ways: the fist group by the fitted variograms and the calculated correlation lengths, while a multi-scale variogram analysis is done for the second group.

Figure 5 shows the calculated correlation length for the facades which variograms reached the maximum variation. The *Generalised Cauchy* [3] models (VESPER 1.6 2006) are fitted through

[3] $\gamma(l_i) = (C0 + C1(1 - rho) \quad , \quad rho = (1 + (l_i/A1)^2)^{\alpha} \quad , (\alpha > 0)$

l_i	...	a horizontal distance
γ	...	fitted variogram
$C0, C1, A1, \alpha$	...	the model coefficients which are calculated in VESPER during the fitting

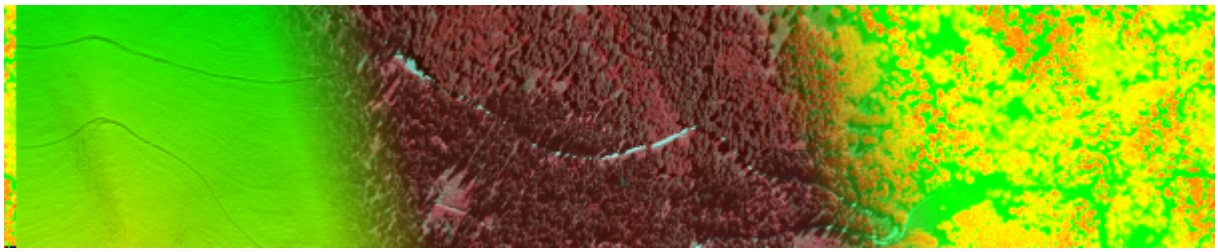

all empirical variograms estimated in this group. Several other models are tried too, but the Cauchy models where the ones with the smallest errors.

It can be seen in the figure that the detrending makes the data less correlated, while the smoothing operator behaves opposite to this. Furthermore, each facade within this group has different sensitivity on the smoothing operator. Facades $M1$ and $M4$ are with similar correlation length values while facade $M2$ has the smallest one in this group.

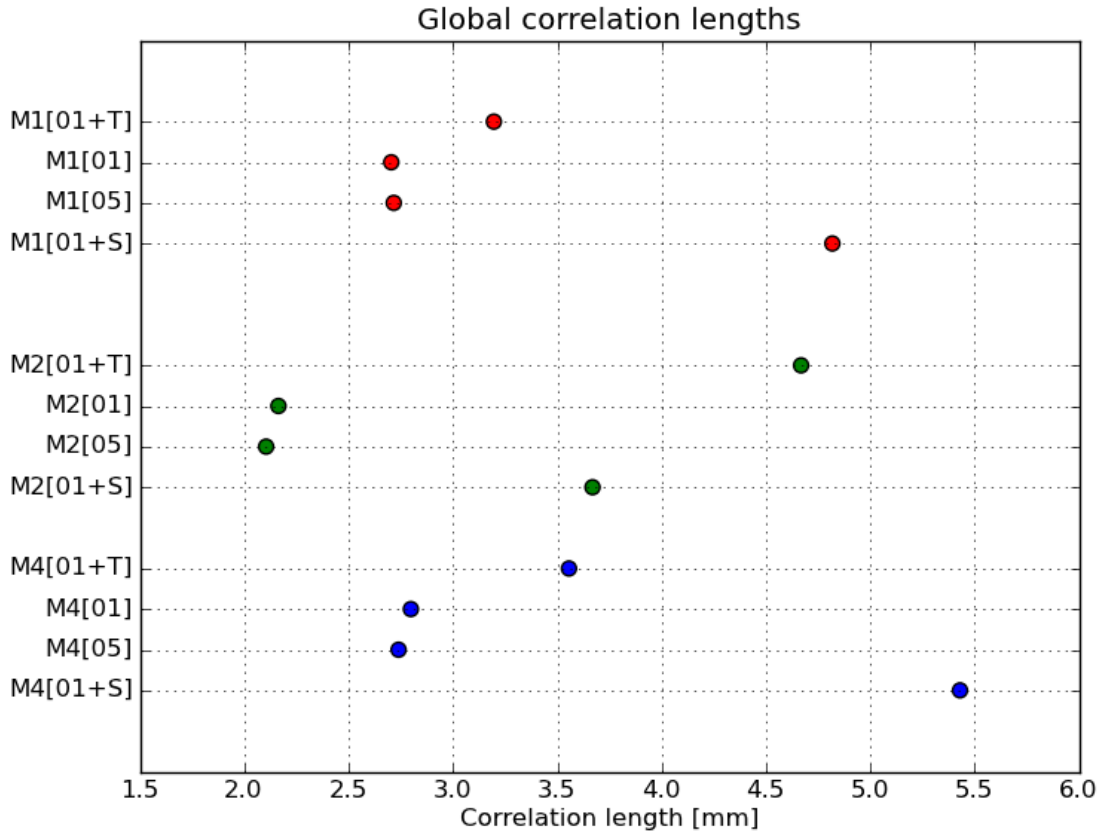

Figure 5: Calculated global correlation length values l [mm] for the first group of the facades.

Figure 6 displays three global variograms calculated for the facade $M3$, that belong to the second facade group. The variograms are different in the maximum lag length which was set at 6, 60 and 180 mm for variograms 6(a), 6(b) and 6(c), respectively. This setting offered a base for a multi-scale analysis.

The variograms from the facade $M3$ have several general characteristics. First, the variograms 6(b) and 6(c) demonstrate several different rates of the data variation over several

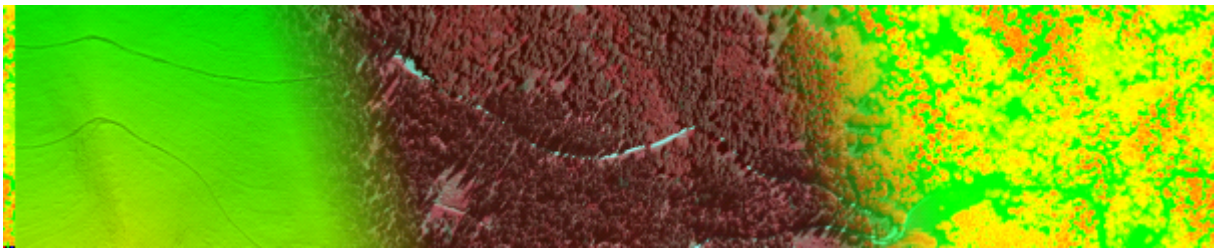

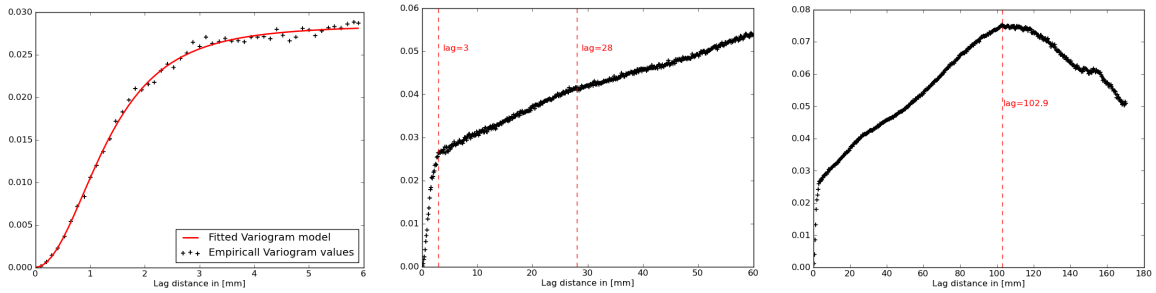

(a) max lag 6mm (b) max lag 60mm (c) max lag 180mm

Figure 6: Three variograms of the facade sample $M3$ calculated based on the [01+T] data set.

horizontal scales. This makes estimation of the global theoretical variogram and the corresponding correlation length very difficult. Second, there is a crucial lag at whom the general trend of data variation is changing. This value is marked with the red dotted vertical line in Figure 6(c). Third, for the data separated up to 60 mm there can be recognised three zones which corresponds to different speeds in data variation. The red dotted vertical lines in Figure 6(b) delineate those zones. Finally, the data shows a local convergence under 6 mm distance which can be seen on the variogram 6(a).

Figure 7 is prepared to aid understanding how the different processing operators affect on the variogram. We can see there that the global data variation is reducing as the detrending and smoothing operators are successively performed. The detrending operator changes the shape of the variogram (especially after lag of $\sim$ 18 mm), whereas the smoothing operator just slightly smooths the variogram almost without changing its shape. Furthermore, it should be noted that zone under lag of 18 mm remains unchanged after the detrending. The variogram from the resampled and detrended data set ([05] DSM) is omitted here because the resampling operator did not significantly affect on it.

In order to compare the facades from the second group with each other we create their global variograms under the maximum lag range (see Figure 8). They are calculated based on the corresponding detrended 0.1 mm grid data sets. We decide to use this data set because its variograms have the smallest 'pollution' due to the processing and therefore, represent the best estimation of the real variograms.

From the Figure 8 we can see that the facade $M6$ appears with a significantly higher variation in heights comparing to the other two. In addition, the facade $M6$ shows two general zones of the data variation: one with an increase and other with an occasionally interrupted decreasing trend. Those two zones are separated at the lag value of 49 mm (see the vertical red dashed line in Figure 8(c)). On the other hand, the facades $M3$ and $M5$ demonstrate only constant increase in the variation and therefore, we can say that the last two did not reach their variation maximums under 180 mm. Nevertheless, there is a local zone in the facade $M3$ variogram that interrupts the general increase.

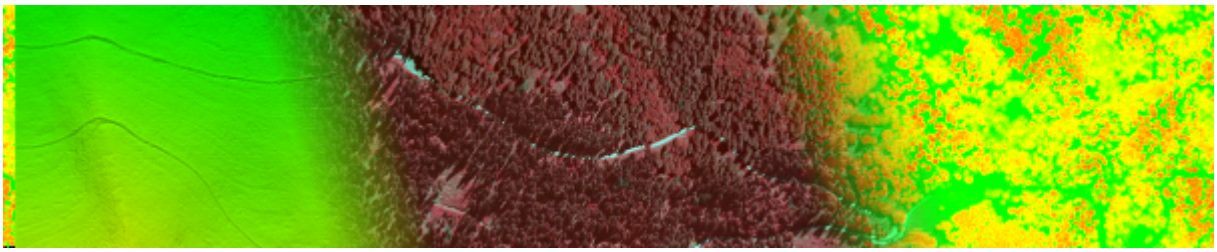

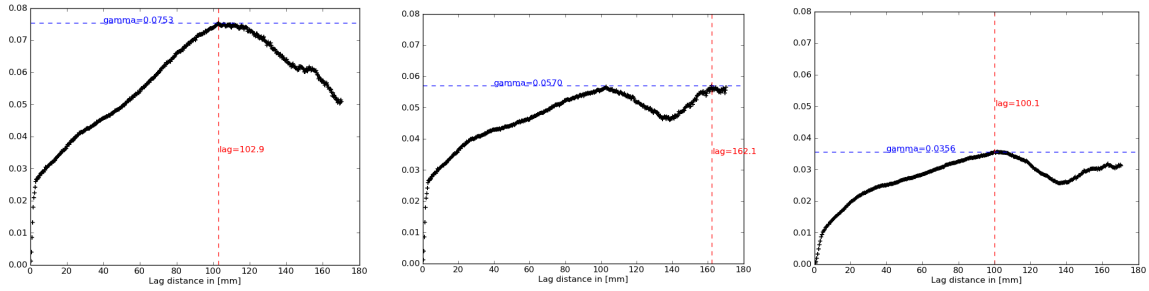

(a) **01+T** data set (b) **01** data set (c) **05+S** data set

Figure 7: Three variograms of the facade sample $M3$ calculated based on the three differently processed data sets.

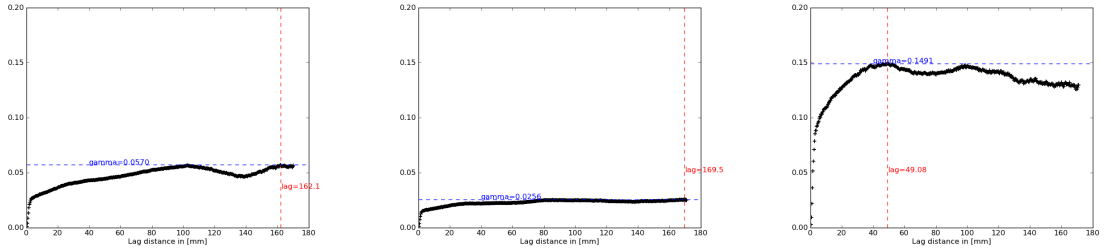

(a) Facade M3 (b) Facade M5 (c) Facade M6

Figure 8: The variograms of the facades from the second group calculated based on the detrended data sets.

Let us now go back at the smoothing operator and analyse it in more details. The graphs in Figure 9 represent the variogram difference of the [05] and [05+S] data sets, calculated for each facade independently. With respect to the variogram definition (Eq.4b) this means that the graphs also are the variograms of the residuals between the [05] and [05+S] surfaces, i.e. the original and smoothed surface. The figures show that for the lags under 2 mm smoothing is extremely low, whilst on the other hand, the smoothing differ over the lags higher that this value. In addition, the residuals for all the three facades are uncorrelated which means that the smoothing operator did not filtered out the trend from the data.

In order to estimate the amount of the performed smoothing we decided to use the mean values from the variograms of the residuals (the horizontal dashed blue line in Figures 9(a),9(b) and 9(c)). It can be seen that the facade $M6$ is the most sensitive on the smoothing; approximately 4.5 and 3 time more than the facades $M5$ and $M3$, respectively (please, note that the axes offsets of Figure 9(c) are different from the other two). This is very much in correlation

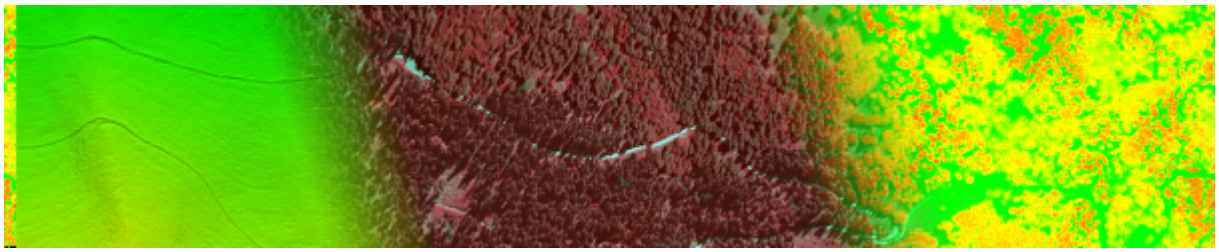

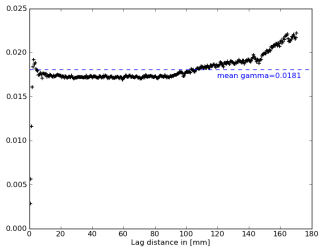

(a) Facade M3

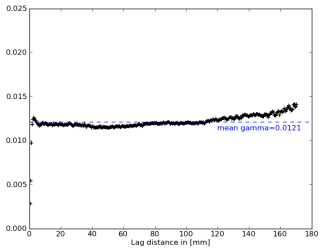

(b) Facade M5

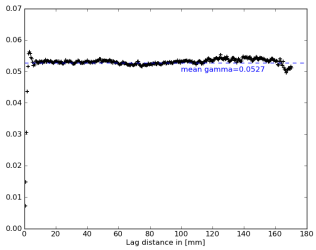

(c) Facade M6

Figure 9: The variograms of the residuals between the original and smoothed facade surfaces.

with the absolute facade variance present in the original variograms (Figure 8). Therefore, it can be said that surface degradation due to the smoothing depends strongly on the starting roughness conditions and dose not manifest uniformly over all the scales.

For the purpose of the multi-scale analysis we estimated the global variograms under the range of 6 mm for the facades from the second group. This zone is characterized by the extremely

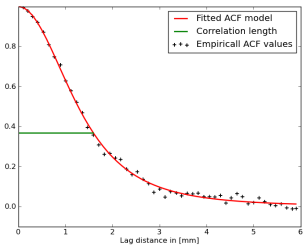

(a) Facade M3

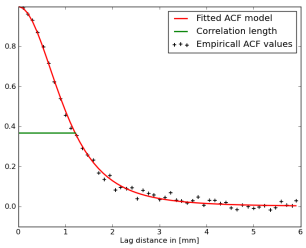

(b) Facade M5

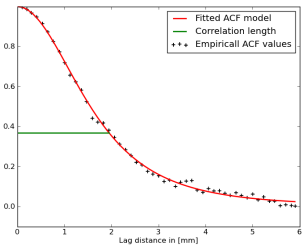

(c) Facade M6

Figure 10: The ACFs of the facades samples from the second group calculated based on the detrended 0.1 mm grid data sets.

high speed of data variation and we decide to estimate it by the corresponding correlation lengths. Therefore, the procedure explained at the beginning of this subsection was performed once more and the corresponding correlation lengths where calculated. Three examples of the fitted ACFs and the calculated correlation lengths are given in Figure 10. They are calculated based on the detrended 0.1 mm grid data sets of the facades from the second group. Similarly as earlier, the correlation length values are summarized in the Figure 11.

The data from Figure 11 confirm once more that the correlation length is highly sensitive to the smoothing operator. However, the results did not show dependence on the detrending which could be due to the very small maximum lag value (6 mm). For the resampling the results show

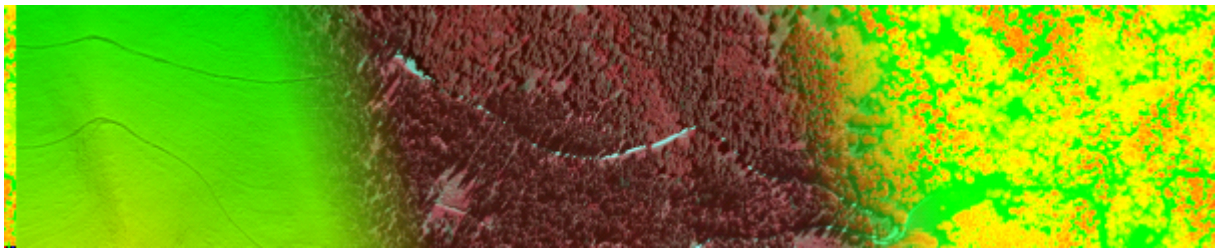

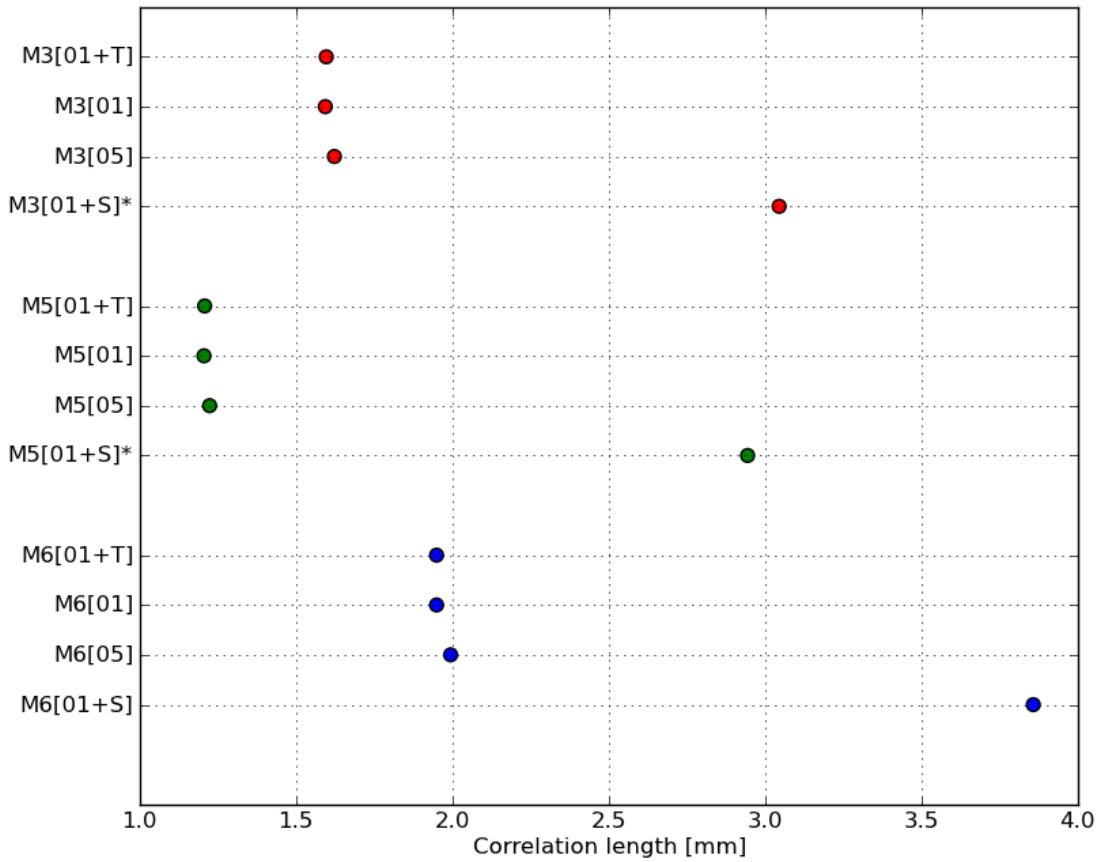

Figure 11: Calculated global correlation length values l [mm] for the second group of the facades. The asterisk symbol stays for the Stable function fitted as an ACF theoretical model. The Cauchy models are fitted for all the other datasets.

little change which can be addressed to randomness of the resampling procedure.

It should be noted that the correlation length values in Figure 11 describe the surface under 6 mm scale and this is a reason why the facade $M6$ has the biggest correlation length. This facade has a low frequency and a high amplitude height fluctuation which under the estimated range appears as a predominantly smoothed surface. On the other hand, the height frequency of the facade $M5$ is under this range and therefore, this surface is highly uncorrelated at this scale.

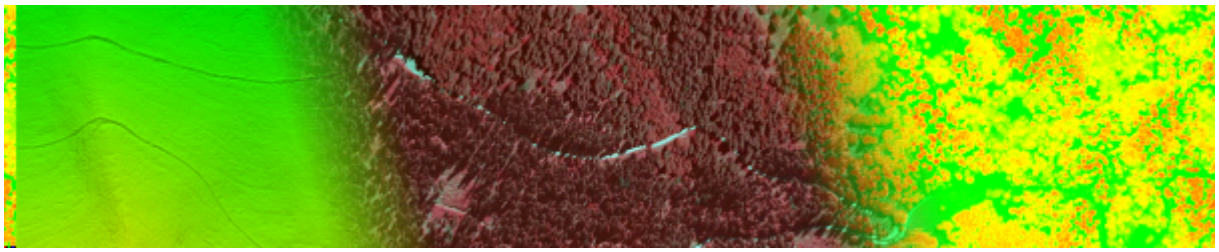

References

Blaes, X. and P. Defourny (2008). Characterizing Bidimensional Roughness of Agricultural Soil Surfaces for SAR Modeling. *IEEE Transactions on Geoscience and Remote Sensing 46*(12), 4050–4061.

Boiffin, J. (1984). *La dgradation structurale des couches superficielles du sol sous l'action des pluies*. Ph. D. thesis, The Institut National Agronomique Paris-Grignon.

Bryant, R., M. S. Moran, D. P. Thoma, C. D. Holifield Collins, S. Skirvin, M. Rahman, K. Slocum, P. Starks, D. Bosch, and M. P. Gonzalez Dugo (2007, January). Measuring Surface Roughness Height to Parameterize Radar Backscatter Models for Retrieval of Surface Soil Moisture. *IEEE Geoscience and Remote Sensing Letters 4*(1), 137–141.

Darboux, F., P. Davy, C. Gascuel Odoux, and C. H. Huang (2002, January). Evolution of soil surface roughness and flowpath connectivity in overland flow experiments. *Catena 46*(2-3), 125–139.

Davidson, M. W., F. Mattia, G. Satalino, T. Manninen, and M. Borgeaud (2000, March). On the characterization of agricultural soil roughness for radar remote sensing studies. *IEEE Transactions on Geoscience and Remote Sensing 38*(2), 630–640.

Helming, K., C. Roth, R. Wolf, and H. Diestel (1993, September). Roughness Mapping on Various Vertical Scales Based on Full-Waveform Airborne Laser Scanning Data. *Soil Technology 6*(3), 273–286.

Hobson, R. D. (1972). Surface roughness in topography: quantitative approach. In R. J. Chorley (Ed.), *Spatial analysis in geomorphology*, pp. 225–245. Methuer, London.

Hoffman, R. and E. Krotkov (1989). Terrain roughness measurement from elevation maps. In *SPIE Vol 1195 Mobile Robols IV*.

Hollaus, M., C. Aubrecht, B. Höfle, K. Steinnocher, and W. Wagner (2011, March). Roughness Mapping on Various Vertical Scales Based on Full-Waveform Airborne Laser Scanning Data. *Remote Sensing 3*(3), 503–523.

Kamphorst, E., V. Jetten, J. Guérif, J. Pitkanen, B. Iversen, J. Douglas, and A. Paz (2000). Predicting depressional storage from soil surface roughness. *Soil Science Society of America Journal 64*(5), 1749–1758.

Kohoutek, T. K. and M. Nitsche (2010). Assesment of flow resistance of steep mountain rivers measuring streambed topography by range imaging technology. *The International Archives of the Photogrammetry, Remote Sensing and Spatial Information Sciences, Commission V XXXVIII*(5), 355–360.

Lievens, H., H. Vernieuwe, J. Álvarez Mozos, B. De Baets, and N. E. Verhoest (2009, February). Error in Radar-Derived Soil Moisture due to Roughness Parameterization: An Analysis Based on Synthetical Surface Profiles. *Sensors 9*(2), 1067–1093.

Linden, D. R. and D. M. Van Doren (1986). Parameters for characterizing tillage-induced soil surface roughness. *Soil Science Society of America Journal 50*(6), 1560–1565.

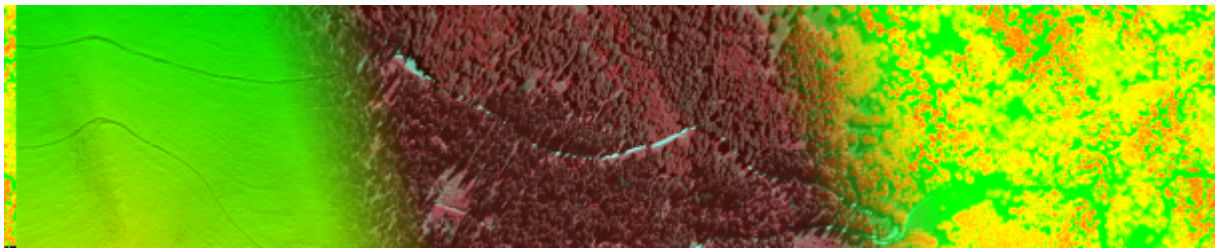

Nikora, V. I., D. G. Goring, and B. J. F. Biggs (1998). On gravel-bed roughness characterization. *Water Resources 34*(3), 517–527.

Perez-Gutierrez, C., J. Martinez-Fernandez, N. Sanchez, and J. Alvarez-Mozos (2007). Modeling of soil roughness using terrestrial laser scanner for soil moisture retrieval. In *Geoscience and Remote Sensing Symposium. IGARSS 2007. IEEE International*, pp. 1877–1880. Ieee.

Smart, G., J. Aberle, M. Duncan, and J. Walsh (2004). Measurement and analysis of alluvial bed roughness. *Journal of hydraulic research 42*(3), 227–237.

Taconet, O. and V. Ciarletti (2007, March). Estimating soil roughness indices on a ridge-and-furrow surface using stereo photogrammetry. *Soil and Tillage Research 93*(1), 64–76.

Verhoest, N. E., H. Lievens, W. Wagner, J. lvarez Mozos, M. S. Moran, and F. Mattia (2008). On the soil roughness parameterization problem in soil moisture retrieval of bare surfaces from synthetic aperture radar. *Sensors 8*(7), 4213–4248.

VESPER 1.6 (2006). User manual. `http://sydney.edu.au/agriculture/pal/software/vesper.shtml`. Online; accessed March 06, 2012.

Whelan, B., A. McBratney, and B. Minasny (2002). VESPER 1.5 SPATIAL PREDICTION SOFTWARE FOR PRECISION AGRICULTURE B.M. Whelan, A.B. M. In P. Robert, R. Rust, and W. Larson (Eds.), *Precision Agriculture, Proceedings of the 6th International Conference on Precision Agriculture, ASA/CSSA/SSSA*, Madison, Wisconsin, pp. 14.

Whitehouse, D. J. (2003). *Handbook of Surface and Nanometrology* (revised and expanded ed.). London: The Institute of Physics.